Neutron diffraction study of USb: The ordered state*

G. H. Lander† and M. H. Mueller
Materials Science Division, Argonne National Laboratory, Argonne, Illinois 60439

D. M. Sparlin
University of Missouri, Rolla, Missouri 65401

Oscar Vogt
Laboratorium für Festkorperphysik, Eidgenössische Technische Hochschule, Zurich, Switzerland

(Received 12 July 1976)

The elastic magnetic neutron cross section from a single crystal of USb has been measured in the antiferromagnetic state (type-I ordering, $T_N = 241.2$ K) for all Bragg reflections with $\sin\theta/\lambda = \kappa/4\pi < 0.811$ Å^{-1}. By using the tensor-operator method, we have calculated the theoretical cross sections from a number of possible ground-state configurations and compared them with experiment. Excellent agreement is obtained for one model only; a $5f^3$ ionic state (U^{3+}) with a $\Gamma_8^{(1)}$ crystal-field ground state. Such a crystal-field ground state implies that the fourth-order crystal-field potential V_4 is negative, which is the opposite sign to that found in the analogous $4f^3$ neodymium compounds. By measuring the temperature dependence of the magnetic scattering as a function of $\vec{\kappa}$, the scattering vector, we have been able to estimate the magnitude of the crystal-field parameters as $V_4 \approx -300$ K, and $V_6 \approx -15$ K. The implications of this first unambiguous identification of the electronic ground state in a metallic actinide compound are discussed.

I. INTRODUCTION

In spite of the considerable research effort undertaken on the actinide monopnictides AX, where A is an actinide ion and X =N, P, As, Sb, and Bi, and monochalcogenides, X =S, Se, and Te, no clear understanding of their electronic structure has emerged.[1] Although no systematic studies of the transamericium compounds have yet been reported, in the heavier actinides, Pu and Am, distinct trivalent-type behavior is evident. In such cases we may use the formalism developed for the corresponding lanthanide systems and consider the interplay between spin-orbit, crystal-field, and magnetoelastic interactions in a well-defined manner. However, in the UX compounds, the situation appears considerably more confusing, and not even the ionization state has been reliably established. We believe these difficulties stem from the extended nature of the $5f$ electrons surrounding the uranium nucleus, and their ability to interact both with the actinide $6d$ electrons as well as with the ligand wave functions. Thus, we find the most perplexing problems in those uranium compounds with the smallest U-U separation,[2] e.g., UN, UP, and US.

In the present study we have measured the elastic neutron cross section from a single crystal of USb. These measurements give information on both the radial extent and the precise composition of the $5f$ wave functions. The availability of relativistic Dirac-Fock wave functions for uranium ions[3] allows us to choose a particular ground-state configuration, calculate the neutron cross section, and compare the results with experiment. We obtain quantitative agreement between theory and experiment for only one of the possible ground-state configurations, which gives us confidence that this is the correct assignment of both the ionicity and the crystal-field ground state of the uranium ions in USb. We have also measured the temperature dependence of the neutron cross section at different values of $\vec{\kappa}$, the scattering vector. By assuming that the magnetic ordering is produced by a simple isotropic molecular field, we have used these measurements to deduce qualitative information about the magnitude of the crystalline electric field acting on the uranium ion.

II. EXPERIMENTAL

A. Previous work

Uranium antimonide (NaCl crystal structure) appears to exist over a range of composition, as indicated by both the lattice parameters (6.176–6.209 Å) and Néel temperatures (217–246 K). Neutron-diffraction studies[4] show the magnetic structure to be type I, which consists of ferromagnetic (001) sheets arranged in the simple +− sequence. The spin direction is perpendicular to the sheets, i.e., $\vec{\mu} \| [001]$. The crystal and magnetic structures are shown in Fig. 1. Values of between 2.2 and $2.8\mu_B$/(U atom) have been reported for the ordered magnetic moment at low temperature.

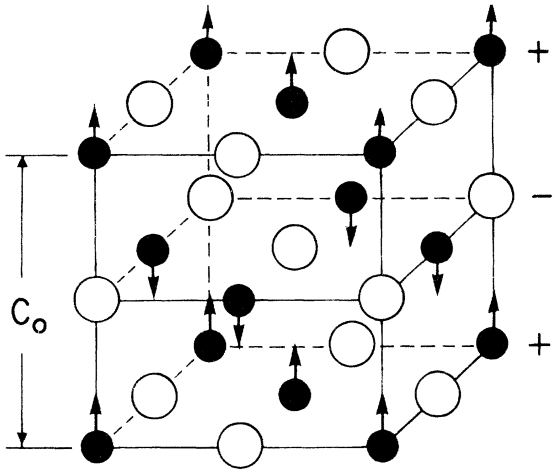

FIG. 1. Uranium antimonide crystal (NaCl) and magnetic (type I) structures. The solid circles are U atoms, the open circles Sb.

B. Crystal preparation

Uranium antimonide crystals were synthesized from high-purity uranium and antimony. A 1-in. bar of uranium was machined on a lathe in an inert atmosphere into turnings of about 0.002 cm diameter. Stoichiometric amounts of uranium and antimony were encapsulated in evacuated silica tubes and held at 600 °C for two weeks. This primary reaction produced a powder mostly consisting of USb. The reaction product was ground and pressed into a $\frac{1}{2}$-in. pellet, which was encapsulated in a sealed tungsten crucible. The crucible was kept for about three weeks at a temperature 50 °C below the melting point of USb with a temperature gradient of 20 °C over the pellet. The resulting recrystallization process produced high-purity single crystals.

C. Experimental procedure

The present experiments have all been performed on a small single crystal of USb with dimensions $2.49\times3.05\times5.46$ mm^3. The experiments were performed at the CP-5 Research Reactor with the cryo-orienter assembly,[5] which is capable of collecting three-dimensional crystallographic data at low temperature. The incident neutron beam ($\lambda=0.992$ Å) was obtained from (311) planes of a Ge monochromator and the $\frac{1}{2}\lambda$ and $\frac{1}{3}\lambda$ contamination was less than 0.01%. The crystal was placed in a small vanadium can in good thermal contact with a copper block containing the heater and calibrated resistors. The temperature was controlled to ±0.1 K. The room-temperature lattice parameter of our USb crystal is 6.197 ± 0.001 Å.

D. Nuclear cross section

To place the coherent elastic nuclear scattering cross section in barns on an absolute scale we define the quantity

$$\left(\frac{d\sigma}{d\Omega}\right)_N = d\sigma_N = |N|^2 \quad \text{(b/mole)}, \tag{1}$$

where N is the nuclear structure factor per molecular unit. For the NaCl crystal structure

$$N_{hkl} = b_U e^{-W_U} \pm b_{Sb} e^{-W_{Sb}}, \tag{2}$$

where the plus sign refers to hkl all even and the minus sign to hkl all odd. The coherent scattering lengths are $b_U = 0.853\times10^{-12}$ cm and $b_{Sb} = 0.564\times10^{-12}$ cm. The Debye-Waller factors, $e^{-W} = \exp(-B\lambda^{-2}\sin^2\theta)$, where B is the isotropic temperature factor and θ is the scattering angle. The integrated intensity is related to $d\sigma_N$ by

$$I_N = C|N|^2 A y/\sin 2\theta, \tag{3}$$

where C is the over-all scale factor, A is the absorption coefficient, and y is the extinction correction. Following Zachariasen,[6]

$$y = (1+2gQ\bar{l})^{-1/2}, \tag{4}$$

where $Q = \lambda^2 V^{-2}|N|^2/\sin 2\theta$, V is the volume of the molecular unit cell, $\bar{l}$ is the effective path length, and g is the extinction parameter.

The intensities of over 400 nuclear reflections were measured at 80 K, sorted into equivalent sets, corrected for absorption, and reduced to average values of N_{hkl}. The values of N_{hkl} were then used in a standard crystallographic least-squares refinement to determine the atomic parameters. The standard deviations were derived from both the counting statistics and the internal consistency within an equivalent set of reflections. The results of such a least-squares refinement with 40 independent N_{hkl} values are

$$C = 30.29\pm0.16, \quad B_U = 0.12\pm0.01 \text{ Å}^2,$$

$$B_{Sb} = 0.11\pm0.01 \text{ Å}^2, \quad g = 2766\pm106,$$

$$R = 0.006 \quad (\chi^2 = 0.8).$$

In this refinement the crystal stoichiometry is fixed at 1:1. If we allow the Sb/U ratio to vary, the value of this ratio is 0.98 ± 0.01. However, with a value of χ^2 already below unity, we cannot justify the additional parameter, and assume that our crystal of USb is stoichiometric.

The extinction corrections for the strong nuclear reflections are appreciable. We illustrate this in Fig. 2 in which $d\sigma_N$ is plotted as a function of $h^2+k^2+l^2$. The data points have not been corrected for extinction. After this correction is made ($g=2766$) the points all lie on the solid lines. For

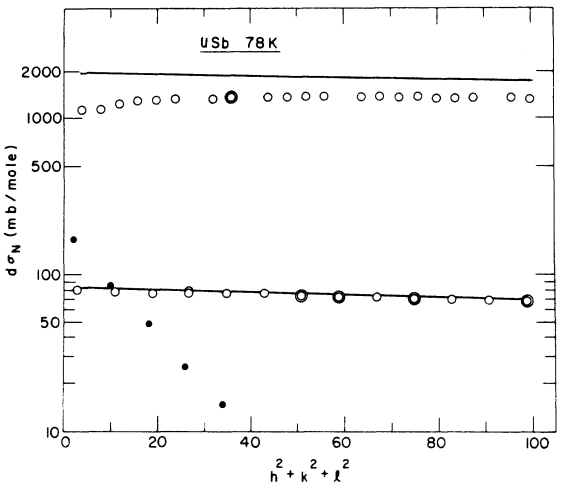

FIG. 2. Nuclear cross sections as a function of the reflection indices $h^2+k^2+l^2$. The open points are uncorrected for extinction. The straight lines represent the least-squares refinement and includes extinction. The solid points are the cross sections for the first five magnetic reflections with $q^2=1$.

comparison we have also plotted the first five magnetic intensities which have $q^2=1$. The intensities fall off rapidly because of the magnetic form factor.

E. Magnetic cross section

The magnetic structure of USb is shown in Fig. 1. The magnetic reflections are indexed on the basis of the chemical unit cell and are such that $h+k=$ even and $h+l=$ odd. Since the magnetic propagation direction of the magnetic structure $\vec{\tau}$ can be parallel to any of the three cubic axes, three types of domains will exist. The magnetic structure factors are such that only one domain contributes at a specific reciprocal-lattice point. We have found no evidence for preferential domain population and have averaged reflections from different domains. The elastic magnetic cross section is given by

$$d\sigma_M = \tfrac{1}{3}q^2|M|^2 \text{ (b/mole)}, \tag{5}$$

where the domain factor is $\frac{1}{3}$, q^2 is the square of the magnetic interaction vector, M is the magnetic structure factor

$$M = 0.2696\times10^{-12}\mu f(\vec{\kappa})\, e^{-W_U} \text{ cm},$$

μ is the magnetic moment per uranium atom in Bohr magnetons, and $f(\vec{\kappa})$ is the magnetic form factor. The intensity of a magnetic reflection then becomes

$$I_M = q^2(\tfrac{1}{3}C)[0.2696\mu f(\vec{\kappa})]^2 \times e^{-W_U} Ay/\sin 2\theta \text{ (b/mole)}. \tag{6}$$

Such a formula relating $f(\vec{\kappa})$ and $d\sigma_M$ is an oversimplification in systems with large orbital moments. Nevertheless, the concept of an effective magnetic form factor is still useful in comparing experiment and theory.

The intensities of 820 magnetic reflections were measured at 80 K and corrected for absorption and extinction (both small effects). Equivalent reflections were averaged and reduced to absolute values of $d\sigma_{obs}$ by using the parameters determined from the nuclear refinements. The values of $d\sigma_{obs}$ are given in Table I. Since $q^2=(h^2+k^2)/(h^2+k^2+l^2)$ the observed values of $d\sigma_{obs}$ can be reduced to $\mu f(\vec{\kappa})$. Comparing experimental and theoretical values for the low-angle cross section gives $\mu = 2.82\pm0.05\mu_B$/(U atom). The experimental values of $f(\vec{\kappa})$ are shown in Fig. 3 and given in Table I.

F. Temperature dependence

To determine the Néel temperature and measure the temperature dependence of the magnetization density we have measured the (110), (223), and (401) reflections at a number of temperatures. The Néel temperature, determined in a separate critical scattering experiment,[7] is 241.2 ± 0.1 K. The reduced temperature plot for the ordered magnetic moment is shown in Fig. 4. The $J=\frac{1}{2}$ and $J=\frac{9}{2}$ Brillouin curves are also drawn.

III. CALCULATION OF THE MAGNETIC CROSS SECTION

No unique determination of the ground-state configuration in an actinide intermetallic system has yet been reported. The first detailed examination of the UX compounds was by Grunzweig-Genossar *et al.*[8] who proposed a $5f^2$ configuration for all compounds. Chan and Lam[1] have proposed a $5f^3$ configuration for the uranium monopnictides, and this model has received further support from the interpretation of high-temperature susceptibility[9] and NMR measurements.[10] In view of the various models, our aim has been to calculate the magnetic cross section from a large number of possible ground states and compare them with the experimental cross section. Previously, this method was applied[3] to the experimental form factor of US, but the lack of appreciable anisotropy in the experimental cross section resulted in some ambiguity in fitting theory and experiment. The large anisotropy observed in the USb cross section (Fig. 3) offers hope that a more definitive assignment can be made in the case of USb.

The magnetic cross section has been calculated with the tensor-operator method.[11] In performing similar calculations for UO_2 we have recently discussed the extension of this method to mixed

TABLE I. Experimental and theoretical results for USb. Only the first 19 reflections are included. A complete table is available from the authors. $d\sigma_M$ is the calculated ($^4I_{9/2}$, $\Gamma_8^{(1)}$ + H_{exch}) cross section. The observed and calculated effective form factors, f_{obs} and f_M, respectively, are determined with Eqs. (5) and (6). Standard deviations in parentheses refer to the least significant digit.

hkl	$\sin\theta/\lambda$ (Å^{-1})	q^2	$d\sigma_{\text{obs}}$ (mb/mole)	$d\sigma_M$ (mb/mole)	$f_{\text{obs}}(\vec{\kappa})$	$f_M(\vec{\kappa})$
110	0.114	1.000	169.1(63)	167.5	0.937(17)	0.9323
201	0.180	0.800	117.2(24)	110.4	0.872(9)	0.8463
112	0.198	0.333	45.8(10)	45.2	0.844(9)	0.8393
221	0.242	0.889	88.7(13)	90.9	0.720(5)	0.7285
310	0.255	1.000	86.6(35)	91.1	0.670(13)	0.6877
203	0.291	0.308	26.3(6)	26.5	0.666(8)	0.6682
312	0.302	0.714	51.9(11)	54.8	0.614(7)	0.6312
223	0.333	0.471	30.1(8)	31.1	0.576(8)	0.5851
401	0.333	0.941	52.3(16)	52.3	0.517(9)	0.5369
114	0.342	0.111	7.3(7)	6.35	0.582(28)	0.5445
330	0.342	1.000	49.2(12)	49.5	0.505(6)	0.5067
421	0.369	0.952	36.3(13)	39.4	0.445(8)	0.4632
332	0.378	0.818	33.0(9)	35.6	0.457(6)	0.4755
403	0.403	0.640	22.7(6)	25.6	0.429(5)	0.4552
314	0.411	0.385	14.8(6)	14.3	0.446(10)	0.4386
510	0.411	1.000	25.8(8)	26.5	0.366(15)	0.3705
205	0.434	0.138	4.1(7)	3.40	0.395(32)	0.3567
423	0.434	0.690	18.3(8)	21.3	0.371(8)	0.4006
512	0.442	0.867	19.8(7)	21.5	0.345(6)	0.3586

J configurations.[12] To calculate the cross section we need to know both the angular and radial terms of the $5f$ wave function. For the radial part of the wave function we use the $\langle j_i \rangle$ integrals given by Freeman *et al.*[3] Our experiments so far have suggested that these radial wave functions are accurate representations of the $5f$ electrons, so that once the number of $5f$ electrons is assigned the values of $\langle j_i \rangle$ are taken as fixed.

The configurations we have considered are listed in Table II. To make meaningful comparisons, the calculated values have been scaled by (μ_{obs}/

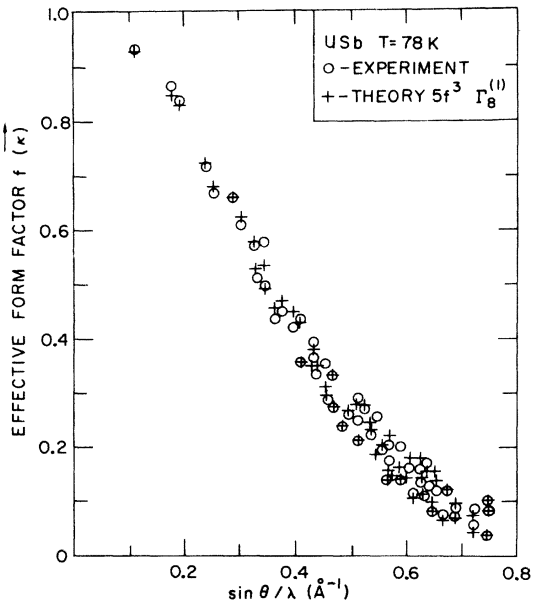

FIG. 3. Effective magnetic form factor for USb. The radial integrals of Ref. 3 have been used together with the $5f^3$ $\Gamma_9^{(1)}$ configuration.

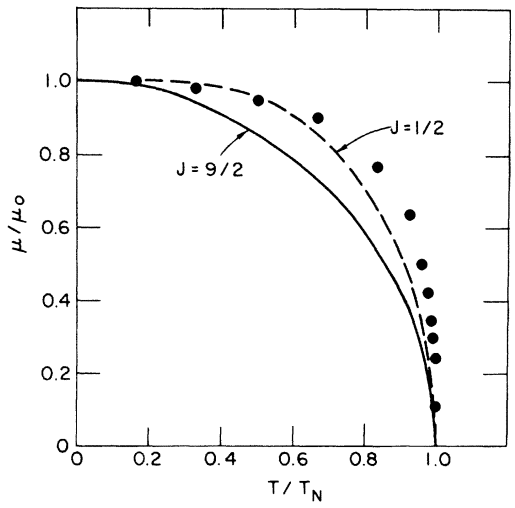

FIG. 4. Reduced magnetic moment as a function of reduced temperature for USb. The Brillouin functions for $J = \frac{1}{2}$ and $\frac{9}{2}$ are also shown.

TABLE II. Wave-function information used in calculating the magnetic cross section of USb. The $|M\rangle$ components are listed. For mixed J configurations the $|M\rangle$ components of each J state are determined by the Γ_i representation and are omitted for brevity. The ionic configurations are single states ($^3H_4$ and $^4I_{9/2}$), intermediate coupling ($J=4$) and ($J=\frac{9}{2}$) as given by Eq. (8), or mixed J configurations (mixed J). The agreement with experiment is indicated by χ^2. The shape prolate is spheroidal, axially symmetric about the axis of quantization, with the long axis being the axis of quantization. The shape oblate is spheroidal with the short axis being the axis of quantization.

Configuration	Crystal-field state	Wave function	μ_{calc} (μ_B)	χ^2	Shape
$f^2\ ^3H_4$	Free ion	$\|4\rangle$	3.20	23.1	Prolate
f^2 ($J=4$)	Free ion	$\|4\rangle$	3.34	34.3	Prolate
$f^2\ ^3H_4$	Γ_5	$0.9354\|3\rangle-0.3536\|-1\rangle$	2.00	15.2	Oblate
f^2 (mixed J)	Γ_5	$0.948\|J=4\rangle+0.194\|J=3\rangle$ $+0.196\|J=2\rangle-0.110\|J=5\rangle$	1.77	19.3	Oblate
$f^3\ ^4I_{9/2}$	Free ion	$\|\frac{9}{2}\rangle$	3.27	44.3	Prolate
f^3 ($J=\frac{9}{2}$)	Free ion	$\|\frac{9}{2}\rangle$	3.42	41.4	Prolate
$f^3\ ^4I_{9/2}$	$\Gamma_8^{(2)}$	$0.791\|\frac{9}{2}\rangle-0.595\|\frac{1}{2}\rangle$ $-0.145\|-\frac{7}{2}\rangle$	2.12	38.0	Prolate
f^3 (mixed J)	$\Gamma_8^{(2)}$	$0.963\|J=\frac{9}{2}\rangle-0.226\|J=\frac{11}{2}\rangle$ $+0.144\|J=\frac{3}{2}\rangle$	1.81	80.3	Prolate
$f^3\ ^4I_{9/2}$	Γ_6	$0.612\|\frac{9}{2}\rangle+0.764\|\frac{1}{2}\rangle$ $+0.204\|-\frac{7}{2}\rangle$	1.33	34.1	Prolate
$f^3\ ^4I_{9/2}$	$\Gamma_8^{(1)}$	$0.968\|\frac{7}{2}\rangle-0.250\|-\frac{1}{2}\rangle$ $-0.011\|-\frac{9}{2}\rangle$	2.36	3.1	Oblate
f^3 ($J=\frac{9}{2}$)	$\Gamma_8^{(1)}$	$0.968\|\frac{7}{2}\rangle-0.250\|-\frac{1}{2}\rangle$ $-0.011\|-\frac{9}{2}\rangle$	2.47	3.9	Oblate
$f^3\ ^4I_{9/2}$ + exchange	$\Gamma_8^{(1)}$	$0.994\|\frac{7}{2}\rangle-0.110\|-\frac{1}{2}\rangle$ $-0.001\|-\frac{9}{2}\rangle$	2.51	2.9	Oblate

$\mu_{\text{calc}})^2$ before evaluating χ^2. Here μ_{obs} and μ_{calc} are the observed and calculated magnetic moments, respectively, and

$$\chi^2=\sum[(d\sigma_{\text{obs}}-d\sigma_M)/\Delta d\sigma_{\text{obs}}]^2/n,$$

where the sum is over all reflections and $\Delta d\sigma_{\text{obs}}$ is the experimental uncertainty on $d\sigma_{\text{obs}}$.

The Hamiltonian for an ion in a crystal may be written

$$H=H_C+H_{\text{so}}+V_{\text{cf}}, \tag{7}$$

where H_C is the Coulomb interaction, H_{so} is the spin-orbit interaction, and V_{cf} is the crystal-field interaction. The strong spin-orbit coupling in actinide ions will mix states of different S and L into the ground-state J manifold. (The so-called intermediate-coupling scheme.) The spin-orbit integral is taken from spectroscopic investigations as 1650 cm^{-1} for uranium in f^2 and f^3 configurations.[1] The resulting wave functions are

$$\begin{aligned} &f^2\text{: } J=4,\quad 0.942|^3H\rangle+0.322|^1G\rangle-0.095|^3F\rangle,\\ &f^3\text{: } J=\tfrac{9}{2},\quad 0.909|^4I\rangle+0.128|^2H_1\rangle-0.397|^2H_2\rangle, \end{aligned} \tag{8}$$

where we have used the notation of Nielson and Koster.[13] We consider the $|M=4\rangle$ and $|M=\frac{9}{2}\rangle$ states for f^2 and f^3, respectively, because in the absence of a strong crystal-field interaction these will be the ground-state wave functions. In Table II the values of χ^2 for both the f^2 and f^3 free-ion configurations, with and without intermediate coupling, show that these calculations do not reproduce the experimental cross section. As we shall see below, this disagreement is primarily because the shape of the magnetization density for both the

$M=|4\rangle$ and $M=|\frac{9}{2}\rangle$ states is different from that found experimentally. All calculations of properties of actinide ions must take into account the strong spin-orbit interaction. However, the wave functions in Eq. (8) are comprised mostly of ^3H and ^4I terms, respectively, which are the Russell-Saunders SL states. Under these conditions, the cross section is not greatly affected by the introduction of intermediate coupling (in fact the χ^2 appear to increase with the mixed SL wave functions) and we may restrict the considerations to a single component.

The next interaction to consider is the crystal field V_{cf}. In a cubic system, this interaction is specified by two parameters defining the fourth- and sixth-order potentials

$$V_4 = A_4\langle r^4\rangle, \quad V_6 = A_6\langle r^6\rangle, \tag{9}$$

where A_4 and A_6 depend on the coordination and surrounding charges and $\langle r^n\rangle$ are expectation values of the $5f$ radial wave functions.[3] All calculations involving the crystal field assume a quantization axis parallel to the cube edge; this is the spin direction in the type-I structure. In the $J=4$ manifold (f^2) the extreme polarization of the Γ_1 singlet and Γ_3 doublet necessary to support a moment in excess of $2.4\mu_B$, leads to essentially free-ion wave functions. In Table II the results are given for the single $J=4\Gamma_5$ triplet as well as for a complete mixed J intermediate-coupling state.[12] Neither calculation fits the experimental cross section. It is apparent that f^2 configurations do not agree with experiment and the remaining calculations concentrate on f^3.

Within a single J manifold the parameters V_4 and V_6 may be conveniently treated by the method of Lea, Leask, and Wolf[14] (LLW). The over-all strength of the crystal field is specified by W and the ratio V_6/V_4 is specified via the parameter x. Thus

$$V_4 = Wx/\beta F(4), \quad V_6 = W(1-|x|)/\gamma F(6), \tag{10}$$

where β, γ, $F(4)$, and $F(6)$ are numerical factors.[14] For the $f^3\,{}^4I_9/2$ configuration

$$V_4 = -57.552Wx, \quad V_6 = -10.446W(1-|x|). \tag{11}$$

Assuming that the crystal-field arises from the nearest-neighbor Sb ions, which are arranged in an octahedral array,

$$V_4 = \tfrac{7}{16}Ze^2\langle r^4\rangle/R^5, \quad V_6 = \tfrac{3}{64}Ze^2\langle r^6\rangle/R^7, \tag{12}$$

where Z is the negative charge at the Sb site at a distance R from the central cation. From Eq. (12) we see that $V_4/V_6>0$, which implies $x>0$ in Eq. (11). Furthermore, we anticipate both from evaluating the terms in Eq. (12) as well as from the results available from lanthanide systems,[15] that the value of $|x|$ is near unity, i.e., V_6 is small. In the calculations that follow we have chosen $x=0.8$; varying x between 0.8 and 1.0 has a negligible effect on the magnetic cross section. The crystal-field interaction acting on the $J=\frac{9}{2}$ manifold leads to two quartets, $\Gamma_8^{(1)}$, $\Gamma_8^{(2)}$, and a Kramers doublet Γ_6. The wavefunctions corresponding to these states are given in Table II. The χ^2 values immediately suggest that neither $\Gamma_8^{(2)}$ nor Γ_6 are correct assignments of the ground state. On the other hand, the $\Gamma_8^{(1)}$ state clearly fits the experimental data well. To further illustrate this we have plotted the effective magnetic form factor in Fig. 3 and given the cross section in Table I.

The important difference between the $\Gamma_8^{(2)}$ and $\Gamma_8^{(1)}$ states as specified here ($x=0.8$) is that the major components are $|M=\frac{9}{2}\rangle$ and $|M=\frac{7}{2}\rangle$, respectively. As indicated in the last column the shape of the magnetization densities are different for these two wave functions. This can be illustrated by focusing on the anisotropy directly. Neglecting the transverse (noncollinear) parts of the magnetization density[12] the effective magnetic form factor is

$$f(\theta,\Phi,\kappa) = \langle j_0\rangle + \sum_{i=2,4,6} c_i\langle j_i\rangle, \tag{13}$$

where c_i are functions of θ and Φ, the polar coordinates relating the direction of the scattering vector and the quantization axis [001] (note that $q^2=\sin^2\theta$), thus $c_i=c_i(\theta,\Phi)$, and the $\langle j_i\rangle$ radial integrals are functions of κ only, $\langle j_i\rangle=\langle j_i(\kappa)\rangle$. The shape of the magnetization density is expressed through the $c_i(\theta,\Phi)$ coefficients. Since both the coefficients c_4 and c_6 and $\langle j_4\rangle$ and $\langle j_6\rangle$ themselves are small, we concentrate on $c_2(\theta,\Phi)$, which varies between 1.7 and 2.0. With a [001] quantization axis, c_2 does not depend on Φ, a consequence of the high symmetry imposed by the cube axis of quantization.[16] If c_2 increases with increasing θ, then the magnetization density is prolate, i.e., it resembles an American football with the moment along the long axis. Conversely, if c_2 decreases with increasing θ, the density is oblate, and resembles a pumpkin with the moment parallel to the compressed axis. One way to choose between these two shapes experimentally is to examine differences between the effective form factors of reflections at the same scattering angle, $\Delta f=f(\vec{\kappa}_1)-f(\vec{\kappa}_2)$, where $|\vec{\kappa}_1|=|\vec{\kappa}_2|$. The open points in Fig. 5 are the experimental values for USb, where $\theta_1<\theta_2$. Since the values of Δf are all positive, c_2 must decrease with increasing θ, and this implies an oblate magnetization density. To provide a quantitative comparison the solid points are calculated values. Considering the small quantity represented by Δf, the fit with $\Gamma_8^{(1)}$ in Fig. 5(a) is

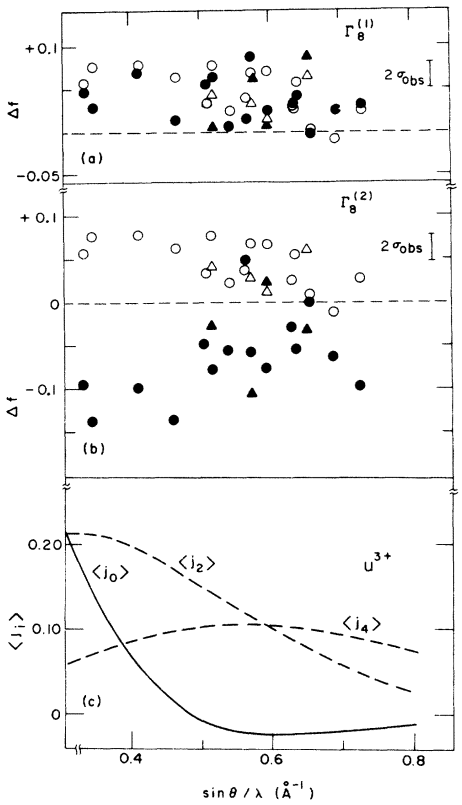

FIG. 5. Anisotropy in the form factor of USb. Δf represents the difference in the form factor between two reflections at the same scattering angle. In cases where more than two reflections occur, different symbols are used. The open points are experimental values. The calculated values for $\Gamma_8^{(1)}$ and $\Gamma_8^{(2)}$ are shown in (a) and (b), respectively. The radial integrals $\langle j_i \rangle$ are plotted for this region of $\sin\theta/\lambda$ in (c).

excellent.

Troc and Lam[9] have fit high-temperature susceptibility measurements on UP and UAs with a model involving a mixed J ground state. (Unfortunately, these authors do not follow the LLW convention and call their ground state $\Gamma_8^{(1)}$. With the values $V_4 \sim 3200$ K, $V_6 \sim 30$ K, as suggested by Troc and Lam, the wave function has a predominant $|M=\frac{9}{2}\rangle$ component and corresponds to the $\Gamma_8^{(2)}$ state of LLW.) The cross section from this wave function is an extremely poor fit to the USb data as shown in Table II ($\chi^2 = 80$). This poor fit is not only because the anisotropy has the wrong sign, but also because the absolute values of $c_2(\theta)$ are reduced by the admixture of $J = \frac{11}{2}$ into the ground state. As a result, the effective form factor falls more rapidly as a function of κ than the experimental data.

One further term must be added to Eq. (7) to represent the internal staggered exchange field that, in the molecular-field model, is responsible for the magnetic ordering. If the exchange is assumed isotropic, then $H_{exch} = \lambda\mu_z$, where λ is the molecular-field constant and μ_z is the projection of the sublattice magnetization on the quantization axis, is added to Eq. (7). In the final row of Table II the $\Gamma_8^{(1)}$ wave function is given when $H_{exch} = 2400$ kOe. This exchange field results in a polarization of the ground state, favoring components with $+M$ values, and increases μ_{calc} from $2.36\mu_B$ to $2.51\mu_B$. With the intermediate coupling g factor this moment becomes $2.62\mu_B$, but is still $0.2\mu_B$ smaller than the experimental value. With the simple models treated here it is not possible to match μ_{obs} and μ_{calc} exactly.

In this section we have demonstrated that the elastic magnetic cross section can give information on the character of the ground-state wave function. The basic approach is analogous to that used in the transition metals, although the computations are more laborious for f electron systems. Since the exchange is very strong in USb, $T_N = 241$ K, the moment is large, $2.82\mu_B$, one might anticipate a free-ion-like situation. This is not the case. Instead, the wave function has a predominant $M = |\frac{7}{2}\rangle$ character that must be a consequence of the strong crystalline-field interaction. If we assume that the octahedral configuration in the NaCl crystal structure determines that $x > 0$, then to produce a $\Gamma_8^{(1)}$ ground state $W > 0$. From Eq. (11) this implies $V_4 < 0, V_6 < 0$. The determination of the strength of this crystalline-field interaction is of fundamental importance to our actinide studies. The most obvious method of doing this, of course, is to measure the energy transitions directly with neutron spectroscopy. Unfortunately, for reasons that are by no means clear, this technique has so far failed to observe transitions between discrete crystal-field levels in actinide systems.[17]

IV. TEMPERATURE DEPENDENCE OF MAGNETIC ANISOTROPY

In an attempt to obtain indirect information about the excited-state wave functions we have measured the temperature dependence of the magnetization density. This method has been applied to iron[18] and holmium.[19] The idea is that as the temperature is raised the exchange field is decreased and, together with the Boltzmann factor, leads to an admixture of higher states into the total wave function. Such higher states lead, of course, to a reduction in the projection of the dipole moment on the quantization axis, but may also lead to a different temperature dependence for the higher (quadrupole, octapole) moments if the excited and ground-state wave functions are of different symmetry. These effects can be observed by the neu-

tron interaction at different values of κ. We have used the simplest model, that of an isotropic exchange field acting on discrete crystal-field states. Since the interpretation of the temperature dependence is a function of the model employed, the qualitative nature of the results should be borne in mind.

In Sec. III we have determined that $W > 0$ for $x = 0.8$. The method of determining the molecular-field constant is then straightforward. First, H_{exch} is added to Eq. (7) and the diagonalization performed for a series of values of W and H_{exch}; the temperature dependence of μ_z being determined each time. The values of W and H_{exch} ranged between 2 and 12 K and between 0 and 3000 kOe, respectively. The eigenvalues for $W = 6$ K are plotted as a function of H_{exch} in Fig. 6. Note the large values of H_{exch}. In low fields the Γ_6 doublet is isotropic, as it must be; at higher fields the upper level interacts strongly with the $\Gamma_8^{(2)}$ states. Figure 7 illustrates the graphical solution for λ with $W = 6$ K. Since the observed magnetic moment of $2.82\mu_B$ is greater than that obtained with the $\Gamma_8^{(1)}$ state at $T = 0$ K, we have plotted the reduced moment on the ordinate axis. The experimental points are plotted by locating the correct isotherm and reduced magnetization value in Fig. 6. If the molecular-field model is valid, the experimental points should lie on a straight line through the origin. The slope of this line determines λ, and the ordering temperature is given by the isotherm that is tangential to the line. As Fig. 6 shows the experimental points do lie on a reasonable line, $\lambda = 920$ kOe/μ_B, and give $T_N \sim 280$ K. Similar plots for other values of W give acceptable solutions for $5 < W < 8$ K, and set limits on λ of $900 < \lambda < 1100$ kOe/μ_B.

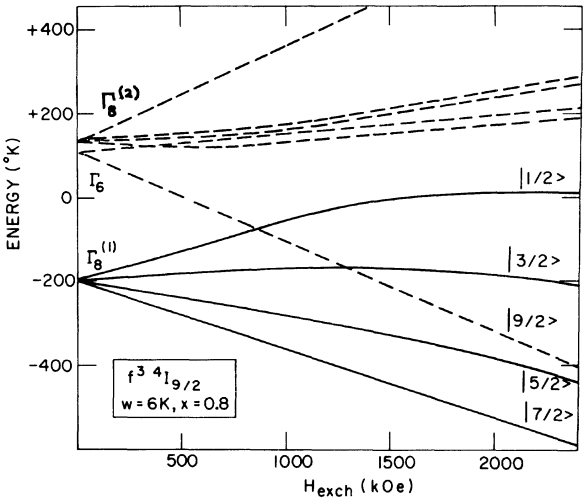

FIG. 6. Variation of the crystal-field levels with internal exchange field. As $H_{exch} \to \infty$ the eigenfunctions tend towards the free-ion states labelled on the right-hand side.

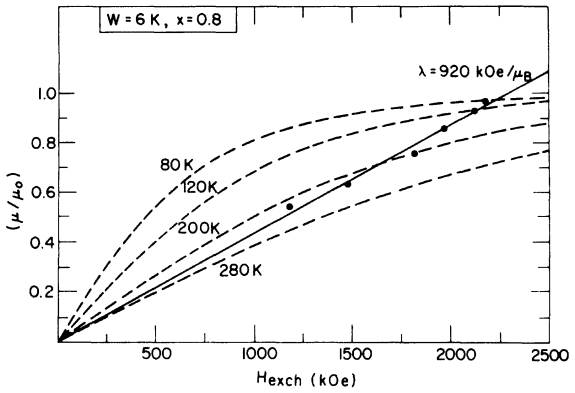

FIG. 7. Determination of the molecular-field constant λ. The experimental points for reduced magnetization are plotted on the isotherms calculated for $W = 6$ K and $x = 0.8$. The straight line through these points and the origin defines λ.

Having obtained a value of λ the experimental value of the reduced dipole moment at any given temperature can be readily reproduced. Simultaneously the magnetic cross section is calculated for all reflections. The quantity of interest here is not the absolute value of the cross section, but the variation in Δf as discussed in connection with Fig. 5. In Fig. 8 the reduced anisotropy in the

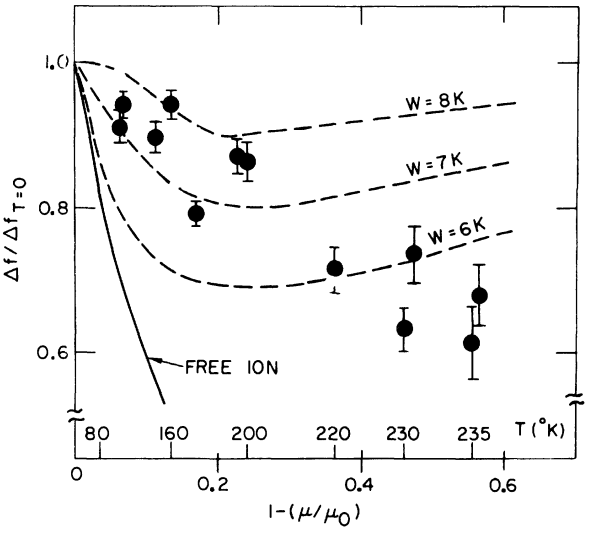

FIG. 8. Temperature dependence of the form-factor anisotropy as determined by the difference between the (223) and (401) magnetic cross sections and plotted as a function of the reduced magnetization. Theoretical values for the free ion ($W = 0$ K) and $W = 6$, 7, and 8 K are shown.

effective magnetic form factor $\Delta f/\Delta f_{T=0}$ is plotted as a function of the reduction in the ordered moment $1-\mu/\mu_{T=0}$, the latter being a function of temperature. The experimental points from two separate runs for the (223) and (401) reflections show some scatter, but $\Delta f_{\rm obs}$ clearly decreases slowly with temperature. These measurements are difficult to make accurately. First, the (223) and (401) reflections are much weaker than the (110), see Table I. Second, as shown in Eq. (13), the form factor contains terms in $\langle j_0\rangle$, $\langle j_2\rangle$, etc. For the (223) and (401) reflections $\kappa=4.18$ Å^{-1} and $\langle j_0\rangle=0.169$, $\langle j_2\rangle=0.213$, and $\langle j_4\rangle=0.066$. The values of Δf arises solely from terms in $\langle j_2\rangle$, $\langle j_4\rangle$, and $\langle j_6\rangle$. The isotropic contribution from the term $\langle j_0\rangle$ simply makes it more difficult experimentally to determine Δf. In the case of spiral magnetic structures the $\langle j_2\rangle$ term can be measured directly.[19]

To calculate the magnetic anisotropy as a function of temperature we first consider the two limiting cases $W=0$ and $W=\infty$. For $W=0$ the situation corresponds to a free ion with the ground state $|M=\frac{9}{2}\rangle$ separated from the next excited state $|M=\frac{7}{2}\rangle$ by an energy determined by the exchange field. Under these conditions the temperature dependence of Δf should be approximately proportional to $(\mu/\mu_0)^{I(I+1)/2}=(\mu/\mu_0)^6$ at low temperatures.[20] Although this linear relationship is modified at higher temperatures, the variation of Δf for $W=0$ is very abrupt, as shown in Fig. 8. Such a rapid variation of the anisotropy with temperature has been observed in holmium.[19] On the other hand, for $W=\infty$ the $\Gamma_8^{(1)}$ state is completely isolated from states of other symmetry and because the cross section is proportional to the square of the quadrupole and higher moments, which are identical for all four $\Gamma_8^{(1)}$ states, the term Δf is *independent* of temperature. This situation occurs in iron, in which the separation of the T_{2g} and E_g states is much larger than the exchange energy.[18] With the present model for USb, Δf is essentially independent of temperature for $W>10$ K. (If $W=10$ K, the $\Gamma_8^{(1)}-\Gamma_6$ separation is ~500 K.) As a first approximation, the temperature dependence of Δf may be associated with the percentage of the $|M=\frac{9}{2}\rangle$ component in the total wave function. The calculated values of $\Delta f/\Delta f_{T=0}$ for $W=6$, 7, and 8 K are shown in Fig. 8. The change of slope at high temperature is associated with the rapid decrease in $H_{\rm exch}$ and the subsequent depopulation of the excited $|M=\frac{9}{2}\rangle$ state, see Fig. 6. In this temperature region the deficiencies of the molecular-field model will be most serious, and it is not surprising that the data do not reflect this change of slope. For example, the molecular-field model overestimates T_N by ~40 K.

V. DISCUSSION

The neutron experiments on USb demonstrate that the ordered-state wave function has a magnetization density that is oblate (see Table II). A detailed comparison with a number of theoretical models shows that the f^3 configuration is the most likely, and that the ground-state wave function must have predominantly $|M=\frac{7}{2}\rangle$ character. As we shall see, this is a most unexpected result. In agreement with the conclusions in our study[12] of UO_2, we have no evidence to suggest that the crystal-field interactions are large enough to introduce the complications of J mixing. To determine the crystal-field ground state we can start by examining the LLW eigenstates for large $|M=\frac{7}{2}\rangle$ components. Possible candidates are $\Gamma_8^{(1)}$ with $0.5<x<1.0$ and $\Gamma_8^{(2)}$ with $x\sim-1$. Since the eigenstates are *identical* for $\Gamma_8^{(1)}$ with $x=1$ and $\Gamma_8^{(2)}$ with $x=-1$, our measurements cannot distinguish between these two alternatives. Initially, it would appear that such an uncertainty in x precludes any detailed statements about the crystal-field parameters. Part of the reason for these difficulties is that in the ordered state the exchange field polarizes the wave functions. Thus, provided the major component in the paramagnetic state is $|M=\frac{7}{2}\rangle$, the strong field will ensure that the coefficient of this state is greater than 0.95 when the moments are fully aligned. Unlike spectroscopic techniques, which measure transitions between the ground and excited states, the form-factor studies sense any wave-function admixture into the ground state (thermally weighted with the Boltzmann factor) by the change in the shape of the magnetization density. To obtain a working model for the electronic structure of USb, we have assumed that the *sign* of the LLW parameter x is defined by the atomic coordination, as suggested by Eqs. (10)–(12). If nearest-neighbor interactions dominate, as we expect, then for the octahedral array in the NaCl structure $x>0$. With this assumption, the ground state is $\Gamma_8^{(1)}$, and to obtain such a ground state both V_4 and V_6 must be negative.

In the NdX series with $4f^3$ electrons, which are the analogous lanthanide compounds,[15] the values of V_4 and V_6 are positive. For NdSb, for example, $x=0.78$, $V_4=84$ K, $V_6=4$ K, and for all the NdX compounds $80<V_4<160$ K. The ground states of these compounds are then $\Gamma_8^{(2)}$ with $|M=\frac{9}{2}\rangle$ as the predominant wave function. Somewhat surprisingly, the simple point-charge model is quantitatively successful in accounting for the crystal-field potentials in the LX compounds.[21] Since the term $\langle r^4\rangle/R^5$ is approximately four times larger in USb than in NdSb, because of the extended nature[3] of the $5f$ electrons and hence larger $\langle r^4\rangle$, we expect

the absolute magnitude of V_4 to be greater in the actinide compound. This is indeed the case. However, the reversal in sign between NdSb and USb is totally unexpected. In terms of an effective point-charge model, it makes no sense to assume the Sb ions have a positive charge. Instead, the conduction electrons (both s and d states) must be considered important factors in determining the electrostatic potential acting on the uranium ion.

By measuring the temperature dependence of the magnetic scattering as a function of $\vec{\kappa}$, we have shown that the shape of the magnetization density changes with temperature. This change of shape (actually a tendency to become more spherical at higher temperatures) is a result of population of excited $|\Gamma M\rangle$ states and can be related to the energy differences between these states. The measurements on USb illustrate that, as expected, the situation is intermediate[1] between that in iron,[18] in which $V_{cf} \gg H_{exch}$, and that in the lanthanide metal holmium,[19] in which $H_{exch} \gg V_{cf}$. Our best estimate is that $V_4 \approx -300$ K and $V_6 \approx -15$ K.

We recognize, of course that other interactions besides an isotropic exchange field play an important role in determining the magnetic properties of USb. Indeed, critical scattering experiments[7] suggest that the exchange interactions are far from isotropic. The absence of transverse critical fluctuations near T_N may require the consideration of strongly anisotropic interactions. Although the crystal-field ground state of USb is $\Gamma_8^{(1)}$, this ground state has a $\langle 111 \rangle$ easy axis of magnetization. Experimentally the spin axis is [001], in apparent conflict with the axis preferred by the crystal field only. A similar situation[22] exists in CeSb and CeBi, for which odd-odd anisotropic interactions have been proposed.[23] One interesting point, for example, is that the agreement between $d\sigma_{obs}$ and $d\sigma_M$ may be further improved to give $\chi^2 = 1.5$ by constructing a $\Gamma_8^{(1)}$ wave function that contains a small admixture of the $|M = \frac{9}{2}\rangle$ state. Within the simple model presented here this cannot be done except by thermally populating the higher states, which then leads to an immediate reduction in the ordered magnetic moment.

In conclusion, the aim of our investigations has been to determine the electronic ground state of USb. Such a determination has important implications for our understanding of the large class of AX compounds, and, indeed, for all actinide intermetallic compounds. To test this model, high-temperature and high-field susceptibility, and inelastic neutron scattering experiments are currently in progress.

ACKNOWLEDGMENTS

We are pleased to acknowledge a number of stimulating discussions with B. R. Cooper and D. J. Lam and wish to thank the former for critically reading the manuscript. The experimental assistance of R. L. Hitterman is greatly appreciated.

---

*Work supported by the U. S. Energy Research and Development Administration.

†Present address: Centre d'Etudes Nucleaires de Grenoble, 38041 Grenoble Cedex, France.

[1]S. K. Chan and D. J. Lam, in *The Actinides: Electronic Structure and Related Properties*, edited by A. J. Freeman and J. B. Darby (Academic, New York, 1974), Vol. 1, Chap. 1; and D. J. Lam and A. T. Aldred, *ibid.*, Vol. 1, Chap. 3.

[2]H. L. Davis, Ref. 1, Vol. II, Chap. 1.

[3]A. J. Freeman, J. P. Desclaux, G. H. Lander, and J. Faber, Jr., Phys. Rev. B 13, 1168 (1976).

[4]M. Kuznietz, G. H. Lander, and F. P. Campos, J. Phys. Chem. Solids, 30, 1642 (1969); J. Leciejewicz, A. Murasik, T. Palewski, and R. Troc, Phys. Status Solidi 38, K89 (1970).

[5]L. Heaton, M. H. Mueller, M. F. Adam, and R. L. Hitterman, J. Appl. Crystallogr. 3, 289 (1970).

[6]W. H. Zachariasen, Acta Crystallogr. 23, 558 (1967).

[7]G. H. Lander, D. M. Sparlin, and O. Vogt (unpublished).

[8]J. Grunzweig-Genossar, M. Kuznietz, and F. Friedman, Phys. Rev. 173, 562 (1968).

[9]R. Troc and D. J. Lam, Phys. Status Solidi B 65, 317 (1974).

[10]D. J. Lam and F. Y. Fradin, Phys. Rev. B 9, 238 (1974).

[11]D. F. Johnston, Proc. Phys. Soc. Lond. 88, 37 (1966); S. W. Lovesey and D. E. Rimmer, Rep. Prog. Phys. 32, 333 (1969); W. Marshall and S. W. Lovesey, *Theory of Thermal Neutron Scattering* (Oxford U.P., London, 1971), Chap. 6.

[12]G. H. Lander, J. Faber, Jr., A. J. Freeman, and J. P. Desclaux, Phys. Rev. B 13, 1177 (1976); J. Faber and G. H. Lander, Phys. Rev. B 14, 1151 (1976).

[13]C. W. Nielsen and G. F. Koster, *Spectroscopic Coefficients for the p^n, d^n, and f^n Configurations* (MIT, Cambridge, Mass., 1963).

[14]K. R. Lea, M. J. M. Leask, and W. P. Wolf, J. Phys. Chem. Solids 23, 1381 (1962).

[15]A. Furrer, J. Kjems, and O. Vogt, J. Phys. C 5, 1381 (1962); P. Bak and P. A. Lindgard, *ibid.* 6, 3774 (1973); A. Furrer and E. Warming, *ibid.* 7, 3365 (1974).

[16]T. O. Brun and G. H. Lander, Phys. Rev. Lett. 29, 1172 (1972); G. H. Lander, T. O. Brun, and O. Vogt, Phys. Rev. B 7, 1988 (1973).

[17]F. A. Wedgwood, J. Phys. 7, 3203 (1974); G. H. Lander, T. O. Brun, B. W. Veal, and D. J. Lam, in *Proceedings of the Montreal Conference on Crystalline Electric Fields in Metals and Alloys*, edited by R. A. B. Devine (University of Montreal, Montreal, 1975), p. 480.

[18]R. C. Maglic, AIP Conf. Proc. 5, 1420 (1972).

[19]G. P. Felcher, G. H. Lander, T. Arai, S. K. Sinha,

and F. H. Spedding, Phys. Rev. B 13, 3034 (1976).
[20]P. A. Lindgård and O. Danielsen, Phys. Rev. B 11, 351 (1975).
[21]R. J. Birgeneau, E. Bucher, J. P. Maita, L. Passell, and K. C. Turberfield, Phys. Rev. B 8, 5345 (1973).
[22]B. R. Cooper and O. Vogt, J. Phys. (Paris) 32, C1-1026 (1971).
[23]B. R. Cooper, M. Landolt, and O. Vogt, *Proceedings of the International Conference on Magnetism, ICM-73, 1973*, edited by R. P. Oserov and Yu A. Izyumov (Nauka, Moscow, 1974), Vol. V, p. 354.